Space and time dependence of the electric field and plasma induced emission in transient and steady-state hollow cathode discharges

M.P. Alberta and J. Derouard*
Laboratoire de Spectrométrie Physique, Université Joseph Fourier (Grenoble I), Boîte Postale 87, 38402 Saint Martin d'Hères Cedex, France

L.C. Pitchford,* N. Ouadoudi, and J.P. Boeuf
Centre de Physique Atomique, Université Paul Sabatier, 118 Route de Narbonne, 31062 Toulouse Cedex, France
(Received 22 February 1994)

We have performed time-resolved observations of the current, optical emission, and electric field profiles in Ar and Ar+1% K hollow cathode discharges. The geometry and pressure are similar to those used in pseudosparks. The discharge was operated with a repetition rate of the order of kHz, an applied voltage in the range 300–600 V and with discharge current up to 1.5 A. Calculations were performed using a 2D, hybrid fluid-particle model developed previously [J.P. Boeuf and L.C. Pitchford, IEEE Trans. Plasma Sci. **PS-19** 286 (1991)]. Good agreement is found between the predictions of the model and the experimental results, and, in particular, both show an initial sharp peak (less than 100 ns in width) in the discharge current a short time after application of the voltage which is related to the expansion of the plasma into the hollow cathode. Further, the model shows that the sequence of events leading to the formation of the hollow cathode discharge is the same in the present experiments and in pseudospark switches operating at much higher voltages.

PACS number(s): 52.80.−s, 52.75.Kq, 52.65.+z

I. INTRODUCTION

Since their discovery at the beginning of this century [1], hollow cathode discharges have been the subject of a large number of studies and have been used in many applications. Recently, there has been an increased interest for *pulsed* hollow cathodes, especially in relation with the development of pseudosparks devices [2–4], which are promising for a number of applications such as fast high power switching and the production of intense electron beams or x rays [5].

The interest in hollow cathodes lies in their large efficiency in terms of current delivered per applied volt. This is largely due to the trapping of energetic electrons in the hollow cathode cavity, resulting in a high ionization rate. These "pendular electrons" [6] are reflected by the cathode fall potential which arises close to the inner walls of the hollow cathode, due to the formation of a space charge electric field inside the hollow cathode volume. Secondary electrons born in ionization events in the high field sheaths are themselves capable of producing further ionization, and this leads to a higher ionization rate than in a similar planar discharge.

The electric field distribution in hollow cathodes was studied experimentally some forty years ago by Little and von Engel [7] who pointed out the existence of the space charge sheaths surrounding the cathode surface.

Recently, the radial distribution of the space charge electric field has been measured in cylindrical hollow cathodes using Stark spectroscopy of the plasma induced emission [8] and the laser optogalvanic effect [9,10]. The knowledge of the distribution of this space charge field is important to understand the transport of the charged particles in the discharge. Its comparison with the results of calculations is a rigorous test for the numerical models.

To date, there exists no experimental measurements of the transient development of the electric field in hollow cathode discharges. This is important in addressing the question of discharge initiation in pulsed hollow cathode discharges and, especially, in the determination of the jitter and delay time in pseudospark discharges for switching applications.

Several authors have observed the space and time dependence of the glow emission in transient hollow cathode discharges [5,11–17]. More recently, capacitive probes have been used to measure the progression of the plasma, which forms first near the planar anode and then propagates towards the rectangular hollow cathode [16]. This is consistent with numerical models [14,18–21] of the initiation phase of triggered pseudospark discharges which show that, at least under certain conditions, a plasma forms near the anode and then propogates, due to ionization events in the volume, towards the hollow cathode [20]. The electron multiplication in the electric field configuration which exists just at the moment the plasma enters the hollow cathode increases by orders of magnitude. This leads to a rapid expansion of the plasma in the hollow cathode volume and a sharp rise in the discharge

*Author to whom correspondence should be addressed.

current.

The purpose of this paper is to provide measurements of the steady-state and transient development of the electric field in transient hollow cathode discharges and to compare these results with model calculations. The electric field was measured using a nonperturbative technique based on laser Stark spectroscopy of NaK molecules introduced as probe molecules in argon discharges [22–24]. The current wave form and the space and time dependence of the emitted light intensity were also measured in the same discharges. Comparisons are made with results from a two-dimensional (2D) hybrid-fluid particle model previously developed [20] to study the initiation phase of pseudospark discharges.

The organization of the paper is as follows. The discharge cell, experimental techniques and conditions are presented in Sec. II, and the numerical model is summarized in Sec. III. The steady-state regime is discussed in Sec. IV where we show the experimentally determined 2D map of the electric field vector. Results in the pulsed regime are presented in Sec. V and further discussed in Sec. VI, where the experimental results are compared with the model calculations and where we argue that the processes that govern the discharge initiation in our low current, relatively low voltage conditions are similar to those that occur in pseudospark discharges at much higher voltages.

II. EXPERIMENT

Experiments have been performed in a discharge cell whose geometry resembles pseudospark devices [2] with transparent walls allowing optical diagnostics. A fast rising (or sometimes dc) voltage is applied between the electrodes. We monitor the corresponding current and voltage wave form together with the space and time-resolved plasma induced optical emission and electric field. The electric field is measured using the Stark effect observed in the laser induced fluorescence spectrum of NaK molecules, present as traces in the gas of the discharge. The experimental setup is similar to previous work [22–24], where additional details can be found.

A. Discharge cell

Three stainless steel, circular, plane parallel electrodes of 58-mm diameter, 1-mm thick (which we shall denote A, K1, and K2, respectively) are contained in a glass envelope (Fig. 1). K1 and K2 are spaced by 10 mm. K1 has a 3-mm diameter central hole and is electrically connected to K2 through four small metal supporting rods. This forms a transparent walled hollow cathode. The anode A is at a distance of 3 mm from K1, corresponding to a situation on the left of the Paschen curve for pressures less than about 1.5 Torr of argon at room temperature. An inner pyrex tube is put on top of K1, around A, to prevent discharge ignition between K1 and the back of A.

The cell is connected to a vacuum system and is filled with argon. For the electric field diagnostic it contains a small amount of Na and K which evaporate as the cell, located in an oven, is heated to about 220 °C. The alkali mixture vapor is in fact mostly composed of K atoms whose relative concentration with respect to the argon buffer gas is typically a few percent [25]. Of course this small percentage is enough to noticeably affect the electrical properties of the discharge gas, due to the large difference in the ionization potentials and excitation cross sections. It also affects considerably the surface properties of the electrodes, even when the cell is not heated (and thus contains only argon in the gas phase). This can easily be seen from the current-voltage characteristics (see below) which show that the breakdown voltage is strongly decreased when the cell has been contaminated by the alkali. However many of the *qualitative* features of the discharges we have observed are similar in both argon and argon-contaminated gases.

B. Electrical setup

1. Steady-state regime

The first experiments with the hollow cathode cell were performed in the steady-state regime. In these conditions we used a stabilized dc power supply, capable of delivering 20 mA at 1 kV, connected to the discharge cell

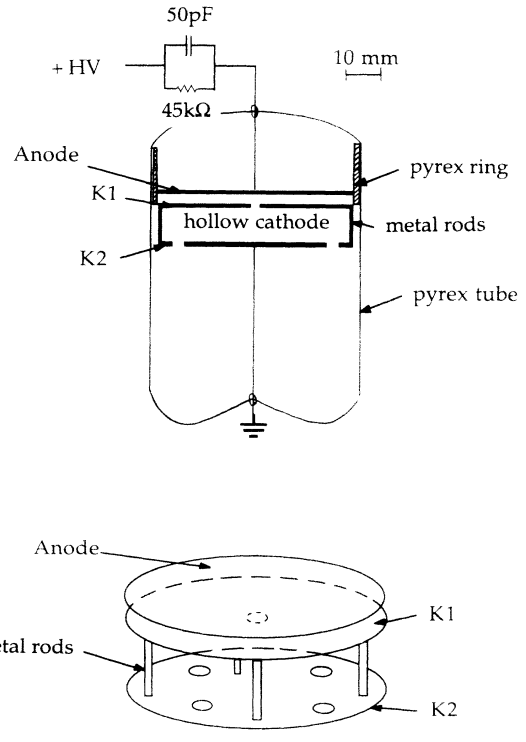

FIG. 1. Schematic of the discharge cell, and its loading circuit. The bottom view shows the electrode construction: four crosspieces form the electrical and mechanical connections between K1 and K2, which allows optical diagnostics.

through a 90 kΩ loading resistor. Current and voltage between the electrodes were measured using a multimeter.

Typically when the cell has not been contaminated by the alkali, the discharge stabilizes at a voltage of about 300 V and a current of 10 mA (with the 90 kΩ loading resistor, this corresponds to the power supply voltage set to about 1.20 kV). The holdoff voltage at a pressure of about 1 Torr of argon is larger than 2 kV, corresponding to a situation on the left of the Paschen curve. The discharge is thus started by producing charges in the cell through the spark formed by bringing a Tesla coil close to the cell.

The effect of contamination of the gas and the electrodes by the alkali can be seen in Fig. 2. After it has been contaminated, the holdoff voltage decreases to about 500 V, the steady-state voltage for the 10-mA current being about 100 V. This voltage does not depend that much on whether the cell is heated or cold; this shows that the composition of the gas (concentration of alkali) is not as important as the surface state of the electrodes, whose surface remains contaminated even when cold.

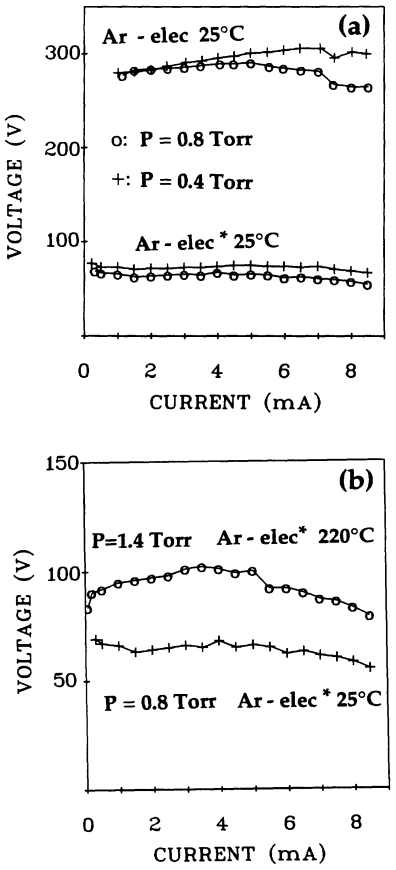

FIG. 2. Current-voltage characteristics of our hollow cathode discharge cell (Fig. 1) in steady-state regime. (a) discharges in pure argon (room temperature), and a comparison between electrodes not contaminated by the alkali (noted "Ar/elec"), and contaminated (noted "Ar/elec*"). (b) comparison between discharges in pure argon (but with alkali contaminated electrodes), and in an argon-0.8% K mixture (oven heated at 220 °C). In this case pressures are chosen so that the gas densities are roughly the same (2.6×10^{16} cm^{-3}).

2. *Pulsed regime*

A pulsed operation is achieved by applying high voltage pulses of about 300 ns rise time, using a homemade, fast electronic switch connected to a high voltage power supply capable of delivering about 1 A rms current at 1 kV. Pulses of about 50 μs are sent at a repetition rate adjustable between 100 and 5000 Hz. A 500 pF capacitance is connected in parallel with a loading resistor (45 kΩ or 90 kΩ): this allows high transient current and voltage, while limiting the rms current to a reasonable value. The intrinsic capacitance of the discharge cell (given by the electrodes geometry) is 23 pF. The voltage wave form is monitored using a 1/100 voltage probe connected to a 7 bit digitizing scope. The wave form of the current circulating between the cathode and the ground is determined by measuring the voltage through a 5-Ω resistor using the same digitizing scope with a 50-Ω termination.

C. Optical diagnostics

1. *Electric field diagnostics*

The laser induced fluorescence of NaK molecules is used to determine the space and time-resolved electric field through the *e-f* Stark mixing effect [26,27]. The laser beam is directed along a diameter of the electrodes. We use for this a single-mode dye laser tuned to the proper NaK ($X\,^1\Sigma^+ - B\,^1\Pi$) transition.

The measurements have been made by exciting $v = 5$ rovibrational levels of the B state, and the values of j were selected from $j = 24$ to $j = 30$, depending of the values of the electric field to be measured [25]. Fields of interest typically range from a few 100 V/cm up to 2 kV/cm. The fluorescence is observed at right angles through a 2-m monochromator. It is detected using a photomultiplier tube (PMT) (Hamamatsu R928) and a photon counting system. For time-resolved experiments, photon counting pulses from the PMT are sent to a homemade digital transient analyzer [22] whose time resolution is usually 100 ns per channel. The transient analyzer is gated by the discharge current spike (see below); Actually, to detect the fluorescence at the very beginning of the breakdown, the photon counting pulses are properly delayed before being sent to the transient analyzer. The signal is accumulated over many cycles (typically about 100 000).

The electric field amplitude is deduced from the Q to R fluorescence line ratio, using calibration curves established previously [25]; its direction is obtained by analyzing the polarization of the fluorescence [23,24].

The discharge cell is mounted on x (radial) and y (axial) translation stages, such that different regions of the

plasma can be successively probed.

An important issue is the size of the probed volume, which determines the spatial resolution. This is determined by the size of the laser beam, by the monochromator slit size, and by the imaging optics. Two configurations have been used:

a. Steady-state experiments. Two-dimensional measurements of the electric field distribution were made as in Ref. [23] by focusing the laser beam to a 0.3-mm diameter waist and imaging the fluorescence along a direction *perpendicular* to the entrance slit of the monochromator which was 0.4 mm wide. With a magnification of the imaging optics of 1, the probed volume is thus rather small, about $0.3\times0.3\times0.4$ mm^3 which results in a very small fluorescence signal. Also it should be noted that when the laser beam is focused, optical pumping and saturation effects are likely to occur which affect the electric field induced spectroscopic signals [27], and, thus, the accuracy of the measurement of the electric field intensity (not the direction, however).

b. Pulsed experiments. In this case, observing fast phenomena at low repetition rate results in a very low signal counting rate per time channel. Consequently, electric field measurements were performed only in the axial y direction and averaged over a region of space whose radial extent is discussed below. In order to increase the signal the laser induced fluorescence was integrated over a length of 10 mm along the laser beam direction. To do this, its image was rotated by 90° so as to be *parallel* to the monochromator slit which was 0.4×10 mm^2. Also, a telescope made with cylindrical lenses was used to expand the laser beam as a ribbon of 10×1 mm^2, which reduces the optical pumping effects and increases the reliability of the electric field intensity measurements. With an aperture of about f/20 the probed volume was roughly included in a slice of 1 mm thickness in the axial y direction of the discharge, and of 10×10 mm^2 in the x and z radial directions.

In conclusion, the electric field measurements in the pulsed discharge regime have been averaged radially over a region from 3 to 13 mm from the axis and centered at about 9 mm off axis of the discharge.

2. *Plasma induced fluorescence*

Different setups have been used to study the plasma induced optical emission.

In a first step, the map of this emission was done by measuring the light intensity detected through a pin hole (diameter 0.5 mm) placed in the image plane (magnification 1) of the discharge. We used for this a PMT (Hamamatsu R928) connected to an electrometer (steady-state regime), or to a digitizing scope triggered by the discharge current (pulsed regime). The measurements were done point by point, moving the pin hole and the PMT in the image plane by steps of 1 mm. Considering the aperture of the optics (about f/10), it is clear that the field depth is comparable to the radius of the discharge (a few cm), and the measured intensity corresponds more or less to a value integrated along the line of sight (z). By contrast, the spatial resolution in the perpendicular directions is less than 2 mm.

In a second run of experiments, time- and spectrally resolved, one-dimensional measurements were made with the same setup previously used for the laser induced fluorescence detection; in these conditions the plasma induced emission was again integrated along the line of sight z, with the resolution in the perpendicular direction x (radial) and y (axial) roughly given by the size of the monochromator slit, corresponding to the volume probed by the laser (see above). In these conditions, both the plasma emission and the electric field can be recorded synchroneously.

III. NUMERICAL MODEL

The basis for the calculations reported here is the two-dimensional, hybrid fluid-particle model reported in Ref. [20]. This model consists of Poisson's equation for the electric field coupled to ion and electron fluid equations for the charged particle transport. The important and distinctive feature of the model is that the ionization source term is determined through a Monte Carlo simulation of the cathode emitted electrons and their progeny from the time they are released from the cathode (assumed to be due to ion bombardment) to the time they are no longer energetically capable of producing further ionization.

The ions are described by the first two moments of the Boltzmann equation, the continuity and momentum transfer equations with the ion flux supposed to be equal to the sum of a mobility term and a diffusion term and the drift and diffusion coefficients being given as functions of the local value of the reduced field, $\mathbf{E}(\mathbf{r},t)/p$ (the local field approximation). The low energy bulk electrons are also represented using a two moment description with the flux equal to the sum of mobility and diffusion terms. The "bulk" electrons determine the electron space charge and the discharge conductivity but do not contribute to the ionization. The electron characteristic energy, the ratio of the electron diffusion coefficient to the mobility, is fixed and equal to 1 eV. As described below, the ionization source term is obtained directly from a particle model, and, thus the assumption of a constant electron characteristic energy has only limited consequences on the results.

Since the ionization source term is an extremely sensitive function of the high energy tail of the electron distribution function and since the electron and ion densities increase exponentially with this source term, it is essential to accurately represent this part of the distribution. Under the low pressure conditions of interest here where the ionization mean free path is on the order or larger than the discharge dimensions, the ionization rate cannot be simply characterized as a function of the local electric field or of the mean electron energy. A good representation of the ionization rate is essential not only for quantitative accuracy, but also for a realistic physical description of the discharge. For these reasons, the behavior of the high energy electrons and, hence, the ion-

ization source term, is obtained, in our model, from a particle (Monte Carlo) simulation. The input to the Monte Carlo simulation consists of the electric field distribution and the distribution of secondary electron current density leaving the cathode surface, and these are determined from the fluid equations. The simulation yields the space dependence of the ionization source term which is, in turn, input to the fluid equations.

The results of the model calculations are the space and time dependence of the charged particle densities and the potential distribution in the discharge volume. From these results, the current wave form and the emission intensity can be deduced. This model was used to elucidate the phenomena occuring during the initiation phase of pseudospark discharges, and the trends predicted by the model are consistent with experiments of the time delay to breakdown [28], with the (indirect) measurement of the progression of the plasma towards the cathode [16], and with recent measurements of the plasma emission during the hollow cathode phase [29]. The measurements here during the discharge initiation, however, provide the most rigorous test of the model predictions. More detail on the physical model, numerical solution technique, and the data in argon are provided in Refs. [20] and [30].

IV. EXPERIMENTAL RESULTS: STEADY-STATE REGIME

A. Plasma induced emission

We discuss first the visual appearance of the discharge in the steady-state regime. The spatial profile of the total emission intensity is shown in Fig. 3 for a discharge in pure argon. Bright emission occurs on the axis in the vicinity of the cathode (K1) aperture. The emission in the main gap (A-K1) is concentrated near the axis but with a radial extent several times larger than the cathode hole radius. No plasma is visible in the main gap (A-K) outside this luminous region close to the discharge axis. By contrast, there is radiation emitted from most of the hollow cathode volume. The radiation in the hollow cathode volume is red on the axis and midway between the electrodes K1 and K2 and blue near the surfaces of the cathode. This latter emission is probably due to the existence of ionic or highly excited states. The red glow in midgap can be due to two-step processes involving the metastable states which would suggest a lower average electron energy in that region. This is consistent with observations of similar discharges in the Ar-K mixtures (see below) where the glow is yellow (associated with emission from low energy excited states in K) on the axis in midgap (K1-K2) while it remains blue near the surfaces of the cathodes.

B. Electric field distribution

These observations are fully consistent with the existence of cathodic sheaths at each electrode inside the hollow cathode, allowing high energy "pendular electrons" [6] to be trapped there and to provide an efficient source

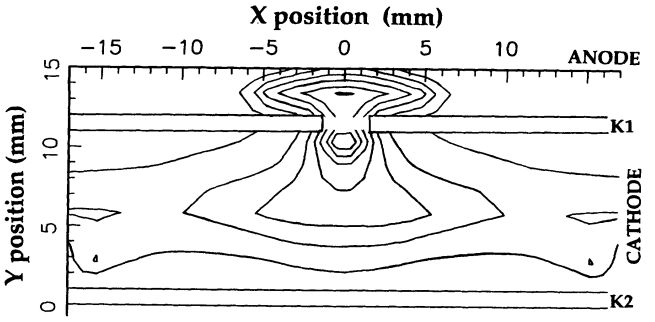

FIG. 3. Contour map of the plasma induced emission of a discharge in pure argon (electrodes not contaminated) in steady-state regime. The emission intensity is integrated over the whole visible spectrum. It is also integrated over the line of sight. Discharge conditions are 7 mA, 304 V, 2.1×10^{16} cm^{-3} (0.65 Torr at room temperature) of Ar.

of ionization. Correlatively a negative glow, a region of very low or zero electric field, develops at mid-distance between the electrodes and, above all, on the axis close to the hole, where a large density of cold electrons and ions concentrates [31]. These cathodic sheaths are associated with space charge electric fields which we have directly measured, as seen on Fig. 4, in a discharge similar to that in the previous subsection, but established in a Ar-alkali-vapor mixture.

We see that an axially uniform electric field exists in the main gap between A and K1, except close to the axis where the field distribution is affected by the space charge created by the plasma. In the hollow cathode volume two sheaths appear close to K1 and K2, separated by an equipotential volume, in agreement with the observations by Little and von Engel [7].

Although the accuracy on the field intensity measurements in these conditions is probably not better than 30% due to optical pumping effects (laser focused), it is enough to claim that the field intensity does not decrease linearly with the distance from the electrode surface: rather, it seems to decrease rapidly over 1 mm close to the sheath edge, from 300 V/cm to below the detection limit, which is less than 100 V/cm for these mea-

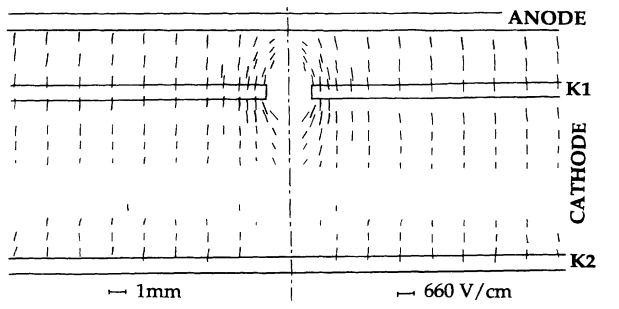

FIG. 4. 2D electric field distribution measured in steady-state regime in a discharge through a Ar-1.8% K mixture. The discharge conditions are 8 mA, 116 V, 1.3×10^{16} cm^{-3} (0.65 Torr at 220 °C).

surements. According to the Poisson equation:

$$\text{div}\mathbf{E} = \frac{\rho}{\varepsilon_0}, \tag{4.1}$$

this indicates an increase of the space charge density at the sheath edge. Such a behavior has been seen in a number of discharges [24,32,33] and is probably correlated with the fact that the ions in the region close to the electrodes are more easily depleted because their velocity is larger due to the higher field. This assumes that the space charge in the electrode sheath is only composed of ions. However, it is conceivable that pendular electrons, moving slowly at the peak of their "swing" could also contribute to the space charge. Actually, numerical simulations [see below and Fig. 5(b)] show that the electron density is negligible in the sheaths.

Although obviously not uniform axially, the field distribution inside the hollow cathode is to a large extent uniform radially, and only very close to the hole is the field distribution distorted by the presence of the relatively dense plasma formed on axis; this is in agreement with the plasma induced emission distribution (Fig. 3), and can be immediately seen by visual inspection of the discharge.

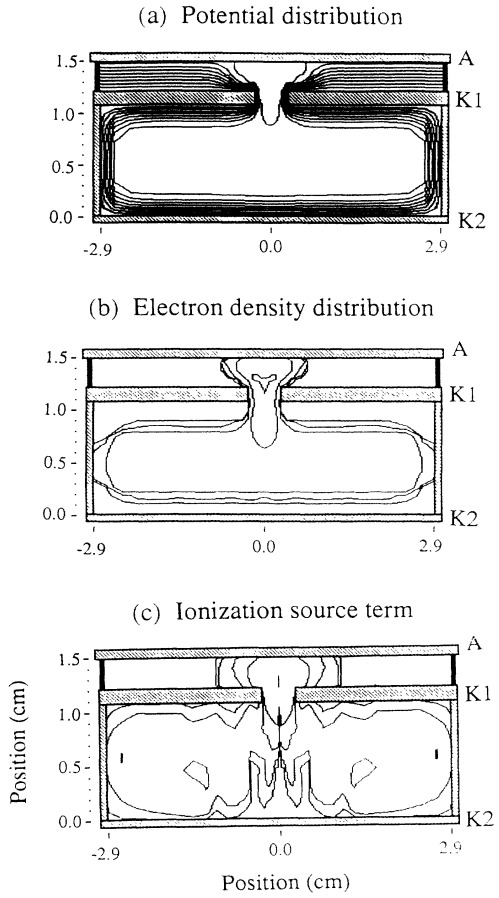

FIG. 5. Quasi-steady-state distribution of (a) potential, (b) electron density, and (c) ionization source term calculated using the hybrid fluid-particle model in argon at 0.65 Torr. The discharge current and voltage are 5.2 mA and 109 V. Ten equally space contours are shown for the potential and the maximum potential in the gap is 112 V. Five contours of constant electron density and ionization source term are shown and these correspond to 0.9, 0.1, 0.01, 0.001, and 0.0001×the respective maximum (1.7×10^{11} cm^{-3} for the electron density and 2.8×10^{17} cm^{-3} sec^{-1} for the ionization source term). The dimensions are shown in units of centimeters.

Figure 5 shows the results of a numerical simulation of a discharge in pure Ar, in conditions similar to the experiment and in the same geometry. We see that the resemblance between the results of the computation and the experimental observation is more than qualitative. This gives us confidence on the validity of the model and on the fact that the discharge in the Ar-K mixture shows a behavior similar to the pure Ar case. Actually, some deviations observed close to the axis between the experimentally measured electric field and the simulation might be explained by the fact that the laser beam was slightly misaligned and did not intersect perfectly the vertical axis of the discharge as it should.

V. EXPERIMENTAL RESULTS: PULSED REGIME

In this section, we shall consider the time evolution of the hollow cathode discharge following the application of a fast rising voltage pulse.

These experiments have been performed in a regime where the discharge is operated in a pulsed, but *repetitive* mode (at a frequency of about 1 kHz). It is probable that there are particles remaining between pulses, and these surviving charges are obviously very important to determine the discharge evolution. In fact, the holdoff voltage can be higher than 2 kV in the steady-state operation, but, once started, the discharge can be ignited repetively at a frequency of about 1 kHz with voltage pulses of only 300 V or less.

A. Current wave form

Figure 6a shows a typical record of the current wave form together with the applied voltage. The current wave form shows three peaks, labeled "0," "1," and "2." The peak "0" corresponds to the charging of the capacitance formed by the discharge cell electrodes as the voltage is applied. It has nothing to do with the glow discharge and appears even when there is no gas in the cell.

The discharge current starts abruptly with a rapidly rising (less than 50 ns in the present conditions) peak ("1"), generally ranging between 20 and 200 mA. It is important to note that this occurs after a delay during which the current is very small (less than 0.1 mA). Although the duration of the delay between the application of the voltage and the beginning of the breakdown is subjected to slow drifts during the course of an experiment, it does not fluctuate from pulse to pulse by more than ±50 ns. The decrease of the current spike "1" is about as fast as its rise. Afterwards the current recovers and increases again, but at a slower rate, with a rise time of

some hundreds of ns. Eventually the current and applied voltage fall off slowly, leading to the broad maximum "2" on the current wave form. If the voltage were maintained at its maximum value for a longer time, the current would continue to grow: this is confirmed by observations performed with no loading resistor, whose results can be seen in Fig. 7.

We have seen the same kind of current wave form over a large range of discharge conditions of pressure, gas composition, electrode surface state, applied voltage (and applied voltage wave form), and repetition rate.

Similar observations have been reported by Störi *et al.* [34].

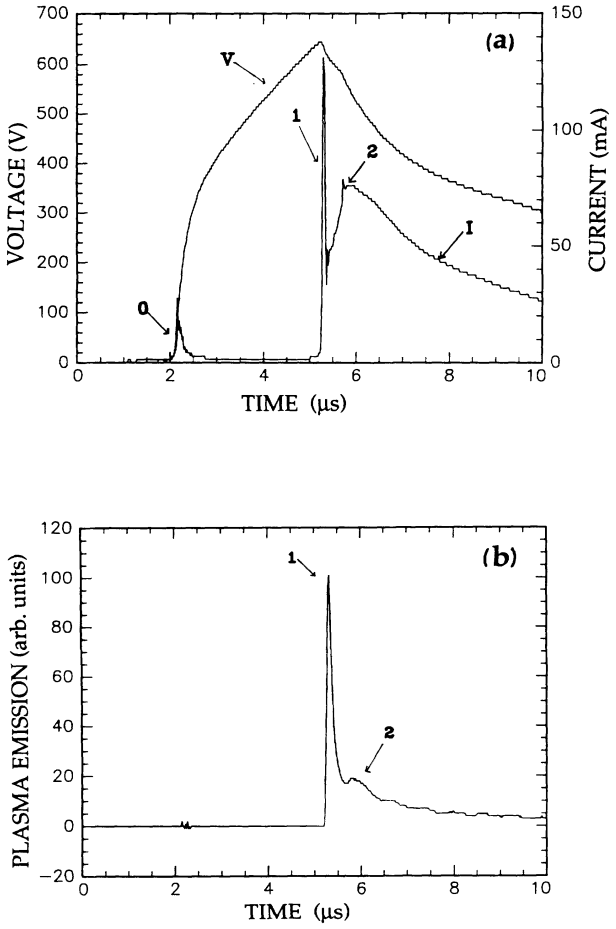

FIG. 6. (a) Current, and voltage, and (b) plasma induced emission wave forms (recorded on the axis between K1 and K2, at 3 mm from the cathode hole) in a pure argon discharge with clean electrodes. The gas density is 3.0×10^{16} cm^{-3} (corresponding to 0.9 Torr at room temperature). The voltage pulses are applied at a repetition rate of 1 kHz. The slower rise of the voltage for $V > 500$ V is due to a small deficiency of the electronic switch. It was corrected for the subsequent experiments shown below (Figs. 7, 9, 11). The labels "0," "1," and "2" refer to different temporal phases of the discharge, as discussed in the text.

1. *Voltage and pressure effects*

Increasing the voltage clearly increases both the current rise time and amplitude as can be seen in Fig. 7. It also decreases the delay between the application of the voltage and the breakdown.

The effect of pressure and voltage can be seen on Fig. 8, which shows that the delay decreases when either the voltage or the pressure increases. Similar observations have been made by other authors [28,35,36].

Concerning the effect of the pressure we can add that the discharge cannot be ignited if the pressure is smaller than about 0.5 Torr. If the pressure exceeds 2 Torr it takes place only in the main gap A-K1 and does not penetrate in the hollow cathode volume. Apart from the delay, the pressure has no simple effect on the current wave form.

2. *Repetition rate effects*

The repetition rate has a very important effect on the delay, as shown by Fig. 9. For a given applied voltage

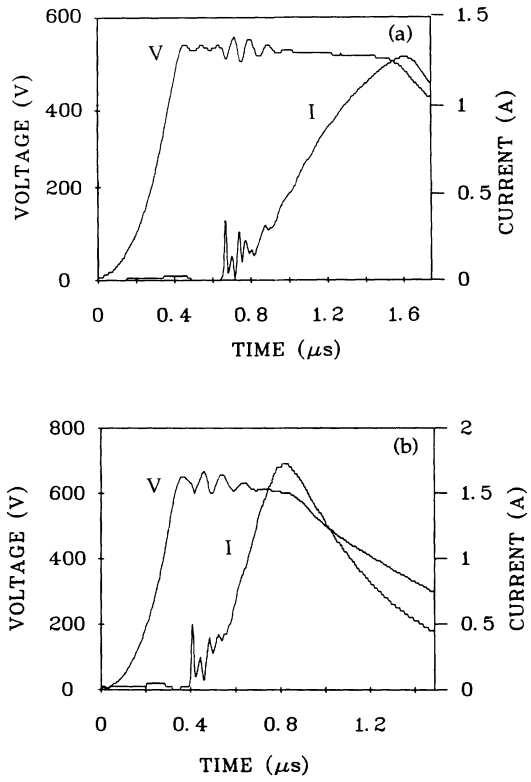

FIG. 7. Effect of the voltage on the current wave form. The gas is pure argon ($1.65\ 10^{16}$ cm^{-3} corresponding to 0.5 Torr at room temperature). The electrodes are contaminated. The voltage pulses are applied at a repetition rate of 1.25 kHz. By contrast with all the other discharge conditions presented in this paper, no loading circuit has been added in series between the high voltage supply and the discharge cell. In these conditions the current can reach an amplitude of about 1.5 A. Afterwards the applied high voltage decreases (because the power supply cannot hold such a current for a long time) and so does the current.

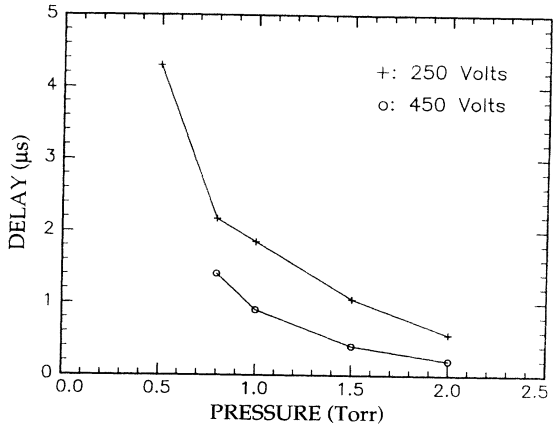

FIG. 8. Effect of the pressure (at room temperature) and of the voltage on the delay between the application of the voltage and the onset of breakdown. The gas is pure argon and the electrodes are contaminated. The voltage pulses are applied at a repetition rate of 1 kHz.

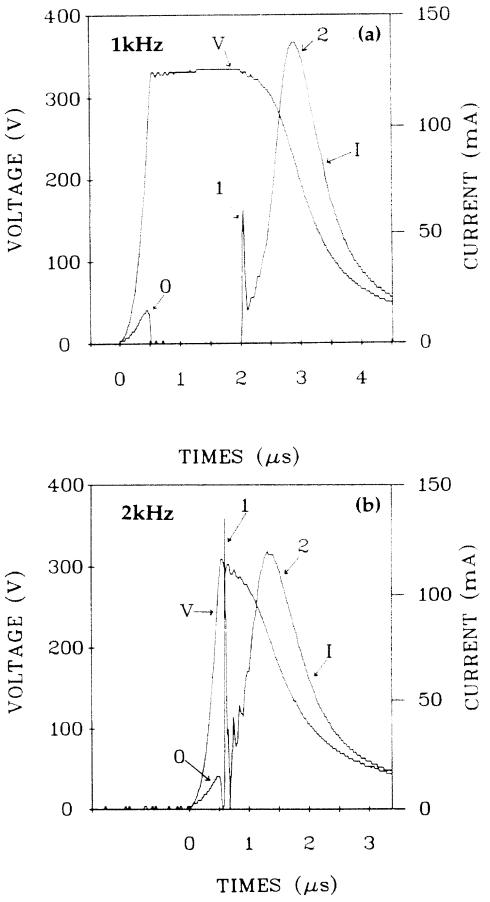

FIG. 9. Effect of the repetition rate on the current wave form. The gas is pure argon (2.6×10^{16} cm^{-3} corresponding to 0.8 Torr at room temperature). The electrodes are contaminated.

and pressure, the delay increases when the repetition rate decreases. The delay can even become infinite (the discharge cannot be ignited) if the repetition rate is smaller than some value, of the order of a few hundreds of Hz. It can be zero, more exactly smaller than the rising time of the voltage, if the repetition rate is larger than a few kHz.

We note also, as can be seen on Fig. 9, that the repetition rate affects the amplitude (and also the width, but to a lesser extent) of the current spike "1," but has little effect on the rising time and amplitude of the broad peak "2."

B. Optical emission

The plasma induced optical emission closely follows the temporal evolution of the current [Fig. 6(b)]. As expected the peak "0" in the current does not correspond to any optical emission. During the delay, the discharge remains completely dark. Although the curve shown in Fig. 6(b) correponds to the emission observed in the hollow cathode volume (between K1 and K2), no emission was detected in the main gap region (between A and K1) during the delay time. Then, the discharge suddenly emits an intense and short flash of light during current peak "1," which again is followed by a slower decrease.

The spatial distribution of the plasma emission is shown on Fig. 10 at two times during breakdown. We see that the flash "1" originates mostly from a strongly localized region just behind the cathode hole in the hollow cathode backspace [Fig. 10(a)], in agreement with previous observations [11,13,14]. Afterwards the plasma

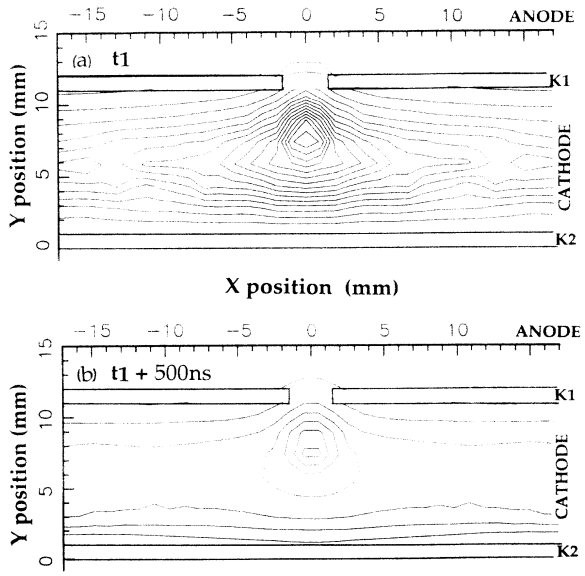

FIG. 10. Time-resolved, plasma induced emission contour maps of the discharge corresponding to Fig. 6. (a) At the breakdown (at peak labeled "1" on Fig. 6). (b) 500 ns later. The maximum intensity is about 400 arbitrary units for (a), with level lines equidistant by 24 arbitrary units. With the same linear scale, the maximum intensity is 65 for (b), with level lines equidistant by 10 arbitrary units.

glow expands and tends to fill the whole hollow cathode volume. Figure 10(b) shows that 500 ns later (peak "2"), the plasma emission is now relatively uniform, apart from the region close to the hole, which remains brighter, and the "sheaths" close to the electrodes. However, the emission intensity close to the hole has fallen considerably, as shown by Fig. 6(b).

C. Electric field measurements

The measurements reported in the preceding sec. V A and V B have been made in the cell filled with pure argon. We will now present results obtained with the cell filled with the argon–alkali-vapor mixture, needed to perform electric field measurements. As shown above, the composition of the gas does not change the behavior of the discharge, whose current wave form [Fig. 11(c)] shows the same overall shape: As before there is a delay between the application of the voltage and the onset of the breakdown which begins by a sharp pulse, followed by a slower increase.

Actually, Fig. 11(c) shows a series of current pulses, the first one — in solid line on Fig. 11(c) — being the most significant: We have found indeed that the appearance of a series of pulses in the current wave form could be correlated with the appearance of a stray discharge beyond the hollow cathode volume through the holes of the back electrode K2 of the hollow cathode (see Fig. 1). The time-resolved monitoring of the plasma induced emission has shown clearly a delay between the emission in the hollow cathode volume, and the emission below K2. This delay is exactly the delay between the first and the second [represented in dashed line on Fig. 11(c)] sharp pulses observed in the current wave form. This indicates that the onset of breakdown in the hollow cathode volume is actually synchronized with the *first* current spike.

Again, as in Fig. 6(b) the plasma emission in the hollow cathode volume [Fig. 11(b)] closely follows the current wave form.

Figure 11(a) shows the electric field wave form recorded at two axial positions in the discharge cell (as deduced from measurements integrated over radial positions from 3 to 13 mm) together with the voltage wave form. The time scales are synchronized with reference to the current and plasma optical emission spikes. We see that the electric field monitored in the main gap closely follows the applied voltage between A and K1, as expected (previous measurements in steady-state, see Fig. 4, have shown there is no space charge in this region). However, we clearly see that no electric field is detected in the hollow cathode before the onset of the current. But the space charge field penetrates suddenly in the hollow cathode as soon as the discharge current rises. Note that the "oscillations" seen in the electric field wave form are not significant (not reproducible). This gives an idea of the uncertainty of the electric field measurement, otherwise difficult to ascertain.

More detailed information about the behavior of the discharge can be seen on Fig. 12 which shows the time evolution of the spatial distribution of the electric field and plasma induced emission along the axial (y) direction in the hollow cathode volume. Recall that the measurements have been integrated radially between 3 and 13 mm from the discharge axis (see Sec. II) so that possible radial nonuniformities may affect the data for times near breakdown, but probably not afterwards (see Fig. 10). We see that the space charge field close to each electrode appears in about 100 ns, and maybe less, as the limited time resolution of our transient analyzer (100 ns/channel) may blur the data. At the same time, we observe the flash of plasma emission which is mostly located at mid-distance between K1 and K2 [Note that the observation volume over which the emission is integrated does not include the axis of the discharge cell: on

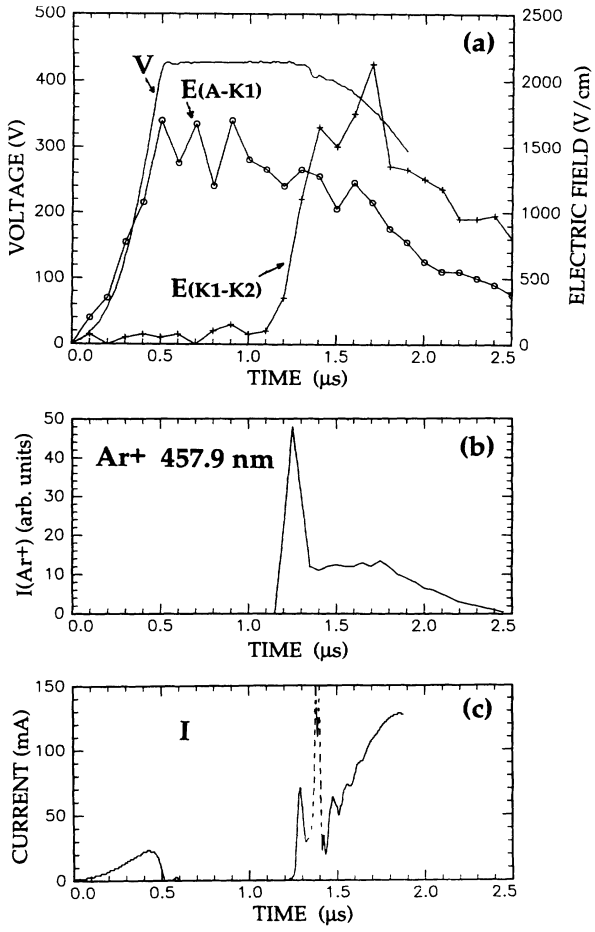

FIG. 11. Current, voltage, electric field, and plasma induced emission wave forms in pulsed regime. (a) Voltage (solid line), and electric field measured in the main gap A/K1 (0), and inside the hollow cathode (+) at 1 mm from K1. (b) Ar^+ emission recorded inside the hollow cathode at mid-distance between K1, and K2. (c) Current wave form. The plasma ignition in the hollow cathode starts at 1.3 μs. The second spike in the dashed line can be associated with a stray discharge (see text). Discharge conditions are 670 Hz repetition rate, 1.8×10^{16} cm^{-3} of Ar-1.3% K (0.9 Torr, 220 °C).

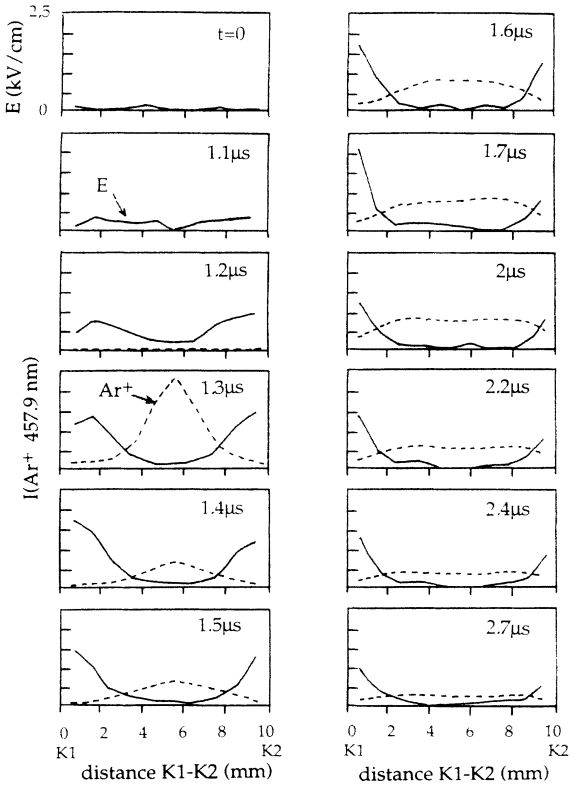

FIG. 12. Space and time variation of the electric field (continuous line) and of Ar^+ (457.9 nm) emission (dashed line) measured in the hollow cathode as a function of the distance between K1 and K2. The measurements are integrated radially over a distance of 10 mm (between 3 and 13 mm from the discharge axis). Discharge conditions are exactly the same as in Fig. 11.

axis, the space distribution of the emission has its maximum closer to the hole, as on Fig. 10(a)]. After the space charge field has developed, the plasma emission spreads closer to the electrodes while the sheaths contract with a characteristic time of a few hundreds of ns, closely related with the rising time of the current (peak "2").

Figure 12 gives also some information concerning the space charge distribution, which is related to the shape of the electric field profile by the Poisson Eq. (4.1). We see that the space charge increases with time as the sheaths contract (the slope of the field profile increases). At time t=1.7 μs, it is about 10^{10} cm^{-3}. Moreover, at the onset of breakdown (times from 1.3 to 1.4 μs) we notice that the net space charge density is not uniform, but increases from the electrodes toward the sheath edge, like in the steady-state regime (Sec. IV, Fig. 4).

VI. COMPARISON WITH NUMERICAL SIMULATIONS AND DISCUSSION

Overall, our experimental results are in good agreement with predictions from the numerical model.

We showed above in Figs. 5 the steady-state potential distribution and the ionization source predicted by the model for a discharge in argon with a current comparable to the experimental results shown in Figs. 3 and 4. The main features seen in the experiment are also found in the numerical results. First, there is a high field sheath surrounding the cathode surfaces. Further, if we suppose that the source term for excitation is roughly proportional to the ionization source term, the spatial dependence of the emission intensity (Fig. 3) can be compared to the calculated ionization source term [Fig. 5(b)]. There is good qualitative agreement between Figs. 3 and 5(b); a maximum in the emission intensity on the axis and near the aperture is observed in both the experiments and in the calculations. Finally, we find that the steady-state, voltage-current characteristic calculated by varying a series resistance is quite flat, in agreement with the experimental results.

It is seen in the comparisons of Figs. 5 that the region in and around the cathode aperture is a negative glow discharge, a low field region which is sustained by energetic electrons accelerated in the high field regions of the discharge and arriving in the negative glow with an energy greater than the ionization potential. Similar to the negative glow in planar discharges, there is a field reversal (due to ambipolar diffusion) which acts to prevent electrons from leaving the glow region [30,37,38], and the charged particle densities are quite high. Since our measurement of the electric field cannot resolve this region and since, at the predicted plasma densities, processes other than those considered in the model (Coulomb collisions, two-step ionization and superelastic collisions) will undoubtedly play a role [39] in this region, we have not paid particular attention to the negative glow region here.

The model predicts a threshold in the initial charged particle densities below which breakdown does not occur. This threshold depends on the discharge conditions and, for the calculations reported here, it is on the order of 10^9 cm^{-3}. Experimentally, as stated above, the discharge does not ignite unless we first introduce some charges into the discharge cell using the spark produced by a Tesla coil. Afterwards, provided the repetition rate is larger than several 100 Hz, the discharge can be reignited with the applied voltage. This critical frequency for reignition is related to the charge density which remains in the gap from one pulse to the next. Also in agreement with the experimental results (Fig. 9), our calculations show that an increase in the initial charged particle densities reduces the delay time and increases the amplitude of the current spike without affecting too much the subsequent evolution of the discharge.

The importance of long-lived excited states in the gas prior to breakdown has been pointed out by a number of authors [31] and recently by Chuaqui *et al.* [40] in the context of pseudospark discharges.

The time evolution of the equipotential contours is shown in Fig. 13 in conditions similar to those in the experiment shown in Figs. 11 and 12. There is a plasma which forms as a result of ionization of the gas by the initial electrons and the secondary electrons emitted from the cathode due to bombardment by the initial ions. This plasma forms first near the anode and then progesses

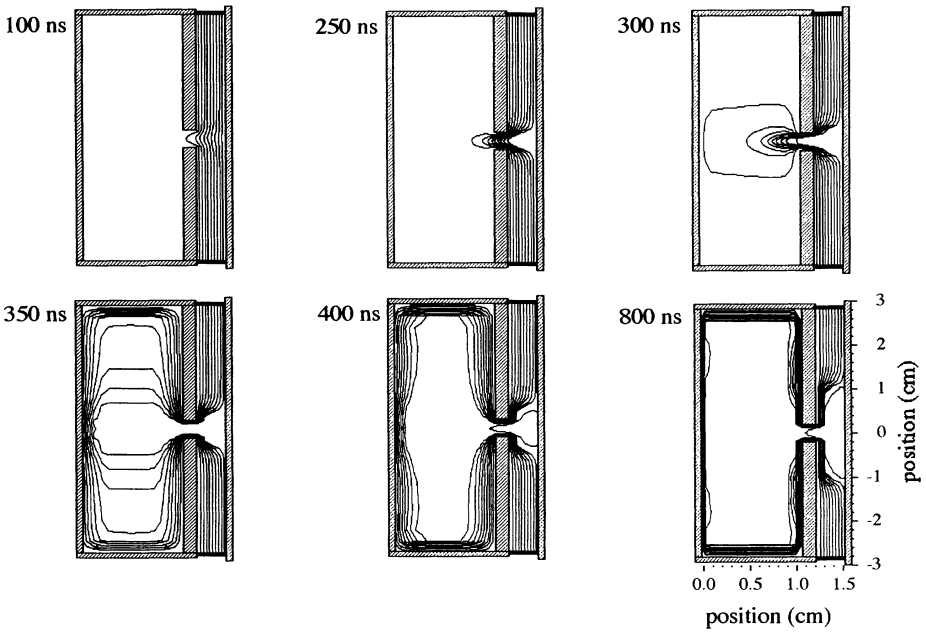

FIG. 13. Equipotential contours during the discharge initiation calculated using the hybrid-fluid particle model, for geometry and discharge conditions similar to the experiment: 0.65 Torr argon; 500 V, constant voltage, applied from $t = 0$ ns.

towards the cathode (due to ionization in the volume) bringing with it the anode potential. This is seen clearly in Fig. 14, which shows the electric field on the axis for different times and these results are consistent with previous calculations using this model at higher voltages [20]. Just at the moment the plasma reaches the hollow cathode, the potential distribution is such that there is a large (several order of magnitude) increase in the electron multiplication which is due primarily to the fact that, in the potential distribution at this time, most of the ionization events occur in the sheaths because of pendulum electrons. (The electron multiplication is the number of electrons created in ionization events in the volume per electron emitted from the cathode.) Hence, the secondary electrons are born in high field regions and they can also contribute to further ionization in the gap. Because of the large multiplication, the plasma rapidly expands into the hollow cathode. The charged particle multiplication decreases again as the plasma expands and pushes the sheaths closer to the electrodes.

The calculated current wave form is shown in Fig. 15, and this is separated into the conduction current at the cathode (ions and cathode emitted electrons) and the total current. The total current wave form is quite similar to that seen in Figs. 6–9 and 11. Following a delay which is on the order of some 100 ns, the current rises suddenly, reaches a peak and then decreases before slowly rising again. The initial current peak is a displacement current at the cathode, and the calculations show that it is due to the changing electric field on the cathode surfaces in and near the aperture (see Fig. 13) as the plasma enters the hollow cathode.

The width of the current peak is related to the time it takes the plasma to make its way into the hollow cathode, and this is quite small since the expansion of the plasma into the hollow cathode is due to the production of charged particles (volume ionization) rather than the transport of charged particles. During this short time, the ions do not have time to move noticeably. Consequently, the conduction current at the cathode, composed

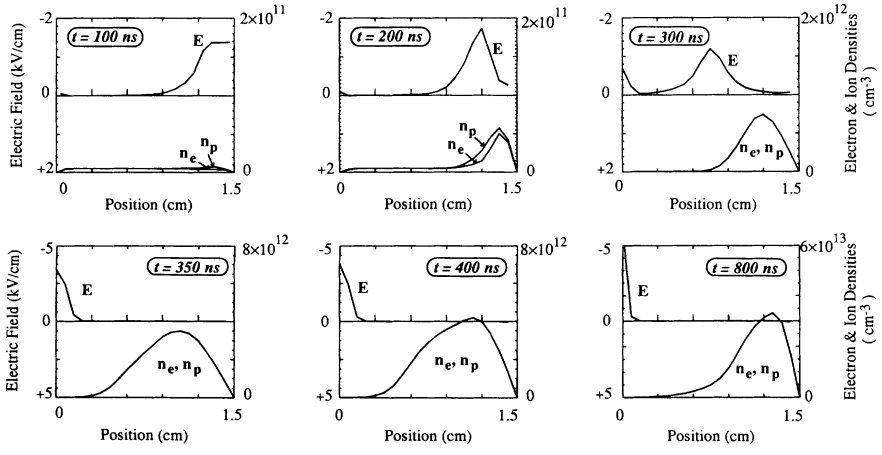

FIG. 14. On axis electric field and charged particle density profiles, at different times during the discharge initiation calculated using the hybrid-fluid particle model. Same conditions as Fig. 13. Note the progression of the plasma from the anode toward the cathode before the current growth.

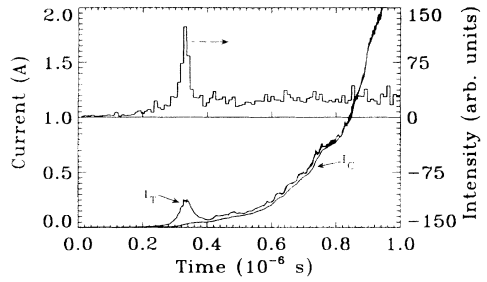

FIG. 15. Total current and conduction current at the cathode calculated using the hybrid-fluid particle model for the same conditions as Fig. 13. Also shown is the source term for excitation (assuming a threshold of 11.6 eV, corresponding to the excitation of Ar atoms from the ground state to the $3p^5 4p$ configuration), integrated over the whole discharge volume.

of the ion current plus secondary electron emission current (possibly induced by photoemission) is very small compared to the total current. The main part of the current at the cathode is actually the *displacement current*, $\mathbf{j}_d$ [Eq. (6.1)] corresponding to the rapid increase of the space charge field:

$$\mathbf{j}_d = \varepsilon_0 \frac{\partial \mathbf{E}}{\partial t} \,. \tag{6.1}$$

This agrees with the experiment (Fig. 12): A variation of the electric field of 2 kV/cm during 100 ns gives a displacement current $\mathbf{j}_d \sim 18$ A/m^2. If we multiply this value by the whole area of K1 and K2 (which is 26.5 cm^2/electrode), this gives a current intensity of about 95 mA, which is of the order of magnitude of the amplitude of the current spike of Fig. 11(c). (This estimation is very crude, in particular because the electric field may not be uniform over the whole radial extent of the electrodes.)

Also shown in Fig. 15 is the excitation rate calculated from the Monte Carlo simulation of an optically allowed transition (threshold at 11.62 eV) as a function of time and integrated over the discharge volume. The favorable configuration of the electric field at the moment the plasma enters the hollow cathode leads to a rapid increase in the multiplication and also in the excitation rates. Thus, consistent with the experimental observations, the peak in the emission intensity is correlated with the first peak observed in the current wave form.

The electron multiplication decreases after the plasma has entered the hollow cathode because relatively less of the ionization events occur in the high field regions and hence the secondary electrons are less effective in producing further ionization. Thus, the current peak reflects the passage of the plasma through the cathode aperture.

After about 400 ns, the *conduction* current at the cathode in Fig. 15 increases and becomes the dominant component of the total current. The subsequent current rise predicted by the model is less than observed experimentally, however. This could be due to approximations in the model such as neglect of two-step ionization or an underestimation of the secondary electron emission coefficient (whose value may be considerably larger than expected [41]).

Figure 16 shows the evolution of the electric field and the emission intensity as a function of axial position for positions off axis (at 6 mm from the axis). These results can be compared directly with the experimental measurements in Fig. 12. Apart from the asymmetry in the calculated emission intensity at 600 ns (which is due to the statistical fluctuations in the Monte Carlo simulation), good agreement with the experimental results can be seen. Because the electron multiplication is always greater than that needed to sustain the discharge, the plasma inside the hollow cathode continues to grow, pushing the sheaths closer to the surfaces of the cathode, as is clearly seen experimentally (Fig. 12) and theoretically (Figs. 13, 14, and 16).

We have already mentioned the fact that increasing the amplitude of the applied voltage leads to a decrease of the delay and to an increase of the rise time of the current. Figure 7 shows clearly that at 600 V of applied voltage the breakdown in the hollow cathode volume occurs in less than 20 ns (watch the width of the first current spike), and that the subsequent current growth is about 1 A/100 ns. This latter is at least 5 times faster than what is observed at 300 V (Fig. 9). This agrees with our numerical simulations [28].

In order to make the connection between the work presented here and pseudospark discharges which normally operate at a higher voltage, we show in Figs. 17 and 18 the calculated current wave forms and emission intensi-

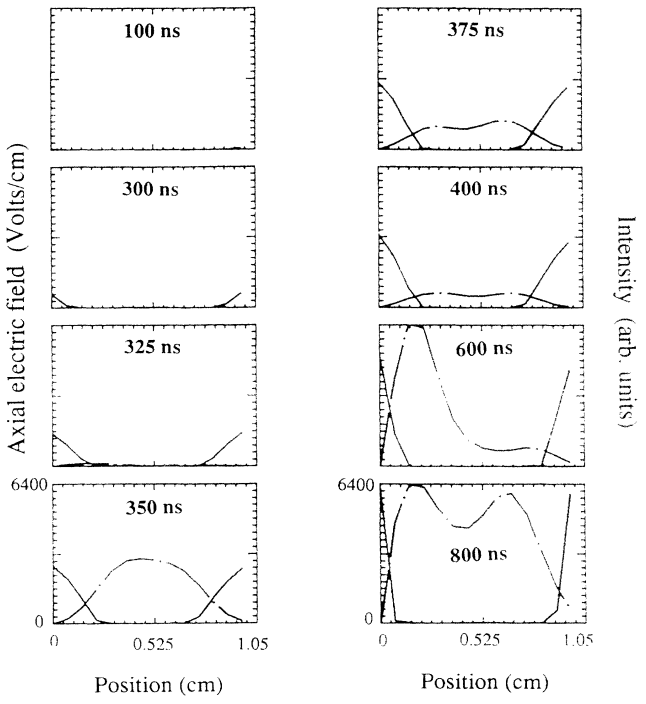

FIG. 16. Time evolution of the electric field (solid line), and of plasma induced emission (dot-dashed line) as a function of axial position for a position 6 mm off axis, calculated using the hybrid-fluid particle model. Conditions are the as Fig. 13. Compare with the experimental results shown in Fig. 12.

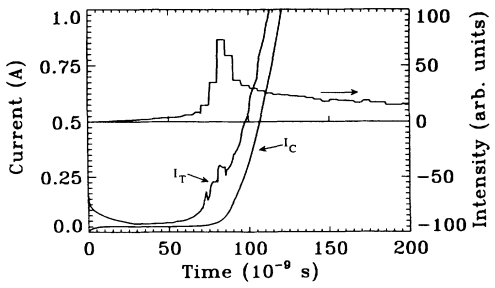

FIG. 17. Calculated wave form of the total current, the conduction current to the cathode, and the ionization rate in He at 0.5 Torr and 2 kV applied voltage. The discharge geometry is described in the text and is similar to the simulations of Figs. 13–16. Note the peak in the displacement current at the cathode (difference between total, and conduction currents), synchronized with the peak in the electron multiplication.

ties during the discharge initiation in helium at 0.5 Torr for applied voltages of 2 and 10 kV. In these calculations, the anode and cathode were symmetrical hollow electrodes, with radii of 1.5 cm and depths of 0.77 cm. The total discharge length was 2.4 cm; the thicknesses of the anode and cathode front plates were 0.2 cm, and the diameters of the electrode apertures were 0.33 cm. These conditions are typical of pseudospark discharges. The evolution of the potential distribution for these two calculations is similar to that reported above; a plasma forms near the anode and expands toward and eventually then fills the hollow cathode volume (see also Ref. [20]). A large increase in the electron multiplication is observed when the plasma enters the hollow cathode, and this appears as a displacement current at the cathode. The distinct peak in the displacement current at early times in the 2-kV current wave form is quite similar to that seen in Fig. 15, but this feature is less distinct in the 10-kV results. From the comparison of Figs. 15–18 and the associated evolution of the potential distribution [30], we conclude that the phenomena occuring during the transient evolution of the low pressure hollow cathode discharges reported here are the same as those occuring during the initiation phase of pseudospark discharges. These results show that the initiation of low voltage hollow cathode discharges is qualitatively similar to that at higher voltages, at least for the conditions of the calculations.

It should be emphasized that the assumptions in the

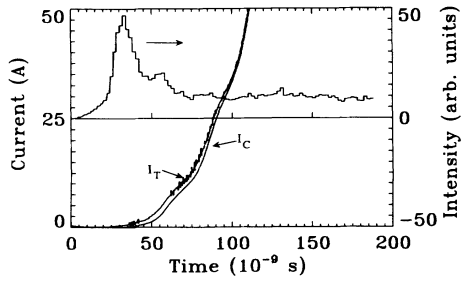

FIG. 18. The same as Fig. 17 but for an applied voltage of 10 kV.

model are valid only for the discharge initiation and hollow cathode phases of pseudospark operation. We have not attempted here to model the transition to the "superemissive phase" [42] where electron emission processes other than secondary emission due to ion bombardment are expected to play an important role.

Finally, in contrast to the calculations reported here where the plasma forms first in the main gap, results from other model calculations [14,18] show the formation of a plasma first on the axis inside the hollow cathode and immediately behind the cathode hole. At higher voltages and for small hole diameters, our model also predicts plasma formation first inside the hollow cathode because the initial charged particles multiply inside the hollow cathode faster than they can be transported into the main gap [28]. The delay and jitter, however, in this cases is quite long. Formation of a plasma inside the hollow cathode can also have deleterious effects on jitter and delay in triggered pseudospark switches unless the conductivity of the main gap is high enough to provide current continuity. In general, this can only be accomplished when there is a plasma in the main gap.

VII. CONCLUSION

We have presented here measurements and comparative calculations of the steady-state and transient electric field distribution and emission intensity in hollow cathode discharges in geometries similar to those used in pseudospark switches. The experiments described here were performed in low current, low voltage discharges for which a spectroscopic diagnostic of the electric field has been developed. Comparative calculations using a two-dimensional, hybrid fluid-particle model are also reported here.

At steady state and in agreement with previous work, we find that the cathode surface is surrounded by a high field sheath which is radially uniform except in the immediate vicinity of the central cathode aperture.

Measurements of the transient evolution of the electric field, the current wave form, and the emission intensity confirm the qualitative predictions of the model, and these are the first results to our knowledge of transient field measurements in hollow cathode discharge. A key point of comparison is the initial peak in the current wave form which is, according to the model, a displacement current on the cathode and which results from the rapid expansion of the plasma into the hollow cathode backspace. This interpretation is supported by the experimental measurements of the time dependent emission intensity which passes through a maximum simultaneously with the initial current spike. The model further predicts that the transient evolution of the electric field distribution in the low voltage discharge studied here is qualitatively the same as that seen in the initiation phase of high voltage, pseudospark discharges.

Most of our experimental results are in good agreement with the numerical model.

ACKNOWLEDGMENTS

This work was initiated as part of a NATO Collaborative Program (Contract No. 900953). We would like to acknowledge the support of the DRET under Contract No. 91-34054. Thanks are also due to J.M. Castejon (IE CNRS) for making and filling the glass cells, and to R. Billat (IR CNRS) for designing and testing the HV switch. The Laboratoire de Spectrométrie Physique is "UA CNRS 08" and the Centre de Physique Atomique is "UA CNRS 277."

[1] F. Paschen, Ann. Phys. (Leipzig) **58**, 731 (1916).
[2] J. Christiansen and C. Schulteis, Z. Phys. A **290**, 35 (1979).
[3] K. Frank, E. Boggasch, J. Christiansen, A. Goertler, W. Hartmann, C. Kozlik, G. Kirkman, C. Braun, V. Dominic, M.A. Gundersen, H. Riege, and G. Mechtersheimer, IEEE Trans. Plasma Sci. **16**, 317 (1988).
[4] For a recent survey, see *The Physics, and Applications of Pseudosparks*, edited by M.A. Gundersen and G. Schaefer (Plenum, New York, 1990).
[5] K. Frank and J. Christiansen, IEEE Trans. Plasma Sci. **17**, 748 (1989).
[6] A. Güntherschulze, Z. Phys. **19**, 313 (1923); Z. Tech. Phys. **11**, 49 (1930).
[7] P.F. Little and A. von Engel, Proc. R. Soc. London Ser. A **224**, 209 (1954).
[8] K. Takiyama, T. Usui, Y. Kamiura, T. Fujita, T. Oda, and K. Kawasaki, Jpn. J. Appl. Phys. **25**, L455 (1986).
[9] C. Hirose, Y. Adachi, and T. Masaki, Appl. Spectrosc. **42**, 815 (1988).
[10] N. Ami, A. Wada, Y. Adachi, and C. Hirose, Appl. Spectrosc. **43**, 245 (1989).
[11] G. Schaefer and M. Wages, IEEE Trans. Plasma Sci. **16** 54 (1988).
[12] W. Hartmann, V. Dominic, G.F. Kirkman, and M.A. Gundersen, Appl. Phys. Lett. **53**, 1699 (1988); J. Appl. Phys. **65**, 4388 (1989).
[13] P. Choi, H. Chuaqui, J. Lunney, R. Reichle, A.J. Davies, and K. Mittag, IEEE Trans. Plasma Sci. **17**, 770 (1989).
[14] K. Mittag, P. Choi, and Y. Kaufman, Nucl. Instrum. Methods Phys. Res. Sect. A **292**, 465 (1990).
[15] E. Wyndham, H. Chuaqui, M. Favre, and P. Choi, Appl. Phys. Lett. **59**, 2231 (1991).
[16] P. Choi, R. Aliaga, B. Blottiere, M. Favre, J. Moreno, H. Chuaqui, and E. Wyndham, Appl. Phys. Lett. **63**, 2750 (1993)
[17] D. Bloess *et al.*, Nucl. Instrum. Methods Phys. Res. **205**, 173 (1983).
[18] H. Pak and M.J. Kushner, J. Appl. Phys. **66**, 2325 (1989).
[19] H. Pak and M.J. Kushner, J. Appl. Phys. **71**, 94 (1992).
[20] J.P. Boeuf, and L.C. Pitchford, IEEE Trans. Plasma Sci. **19**, 286 (1991).
[21] B.M. Penetrante and J.N. Bardsley (unpublished).
[22] H. Debontride, J. Derouard, P. Edel, R. Romestain, and N. Sadeghi, Phys. Rev. A **40**, 5208 (1989).
[23] M.P. Alberta and J. Derouard, J. Phys. D **24**, 904 (1991).
[24] M.P. Alberta, H. Debontride, J. Derouard, and N. Sadeghi, J. Phys. III **3**, 105 (1993).
[25] J. Derouard, H. Debontride, T.D. Nguyen, and N. Sadeghi, J. Chem. Phys. **90**, 5936 (1989).
[26] C.A. Moore, G.P. Davis, and R.A. Gottscho, Phys. Rev. Lett. **52**, 538 (1984).
[27] J. Derouard and N. Sadeghi, Opt. Commun. **57**, 239 (1986).
[28] L.C. Pitchford, N. Ouadoudi, J.P. Boeuf, M. Legentil, V. Puech, C. Thomaz, and M. Gundersen, J. Appl. Phys. (to be published); N. Ouadoudi, thesis, Université Paul Sabatier, Toulouse, 1994.
[29] M. Gasiel, A. Heiligtag, H. Hillmann, F. Müller, H. Wentz, and J. Westheide (unpublished).
[30] A. Fiala, L.C. Pitchford, and J.P. Boeuf, Phys. Rev. E **49**, 5607 (1994).
[31] A. von Engel, *Ionized Gases* (Clarendon, Oxford, England, 1965).
[32] R. Warren, Phys. Rev. **98**, 1650 (1955).
[33] R.A. Gottscho, Phys. Rev. A **36**, 2233 (1987).
[34] H. Störi, T.D. Märk, R.N. Varney, and M. Pahl, Beitr. Plasma Phys. **18**, 79 (1978).
[35] W. Hartmann, G. Bittner, J. Christiansen, K. Frank, N. Lieser, C. Schulteiss, and W. Steudner, Physikalisches Institut, Universität Erlangen-Nurnberg, Research Report No. 8, 1981 (unpublished).
[36] M. Favre, A.M. Lenero, P. Choi, H. Chuaqui, and E. Wyndham, Appl. Phys. Lett. **60**, 6 (1992)
[37] E.A. Den Hartog, D.A. Doughty, and J.E. Lawler, Phys. Rev. A **38**, 2471 (1988).
[38] R.A. Gottscho, A. Mitchell, G.R. Scheller, Y.-Y. Chan, and D.B. Graves, Phys. Rev. A **40**, 6407 (1989).
[39] J.E. Lawler, E.A. Den Hartog, and W.N.G. Hitchon, Phys. Rev. A **43**, 4427 (1991).
[40] H.H. Chuaqui, M. Favre, E. Wyndham, L. Arroyo, and P. Choi, IEEE Trans. Plasma Sci. **17**, 766 (1989).
[41] C. Böhm and J. Perrin, Rev. Sci. Instrum. **64**, 31 (1993).
[42] A. Anders, S. Anders, and M. Gundersen, Phys. Rev. Lett. **71**, 364 (1993).